Fast Capture, Collection, and Targeted Transfer of Underwater Gas Bubbles Using Janus-Faced Carbon Cloth Prepared by a Novel and Simple Strategy

Haniyeh Tahzibi, Saeid Azizian, Sabine Szunerits, Rabah Boukherroub

ACS APPLIED MATERIALS & INTERFACES

www.acsami.org Research Article

Fast Capture, Collection, and Targeted Transfer of Underwater Gas Bubbles Using Janus-Faced Carbon Cloth Prepared by a Novel and Simple Strategy

Haniyeh Tahzibi, Saeid Azizian,* Sabine Szunerits, and Rabah Boukherroub

Cite This: https://doi.org/10.1021/acsami.2c12027 Read Online

ACCESS | Metrics & More | Article Recommendations | Supporting Information

ABSTRACT: Transportation of bubbles in liquids in a controlled fashion is a challenging task and an important subject in numerous industrial processes, including elimination of corrosive gas bubbles in fluid transportation pipes, water electrolysis, reactions between gases, heat transfer, etc. Using superaerophilic surfaces represents a promising solution for bubble movement in a programmed way. Here, a novel and low-cost method is introduced for the preparation of Janus-faced carbon cloth (Janus-CC) using poly(dimethylsiloxane) (PDMS) coating and then burning one side of the carbon cloth/PDMS on an alcoholic burner. The results show that the superhydrophobic face behaves as a superaerophilic surface, while the superhydrophilic side is aerophobic underwater. Subsequently, the Janus-CC is applied for pumpless transport of underwater gas bubbles even under harsh conditions. The movement of gas bubbles on the surface of the Janus-CC is interpreted based on the formed gaseous film on the aerophilic side of the Janus-CC. Various applications of the prepared Janus-CC for underwater bubble transportation, such as underwater gas distributor, gas collector membrane, gas transport for chemical reactions, unidirectional gas membrane, and elimination of gas bubbles in transport pipe, are presented.

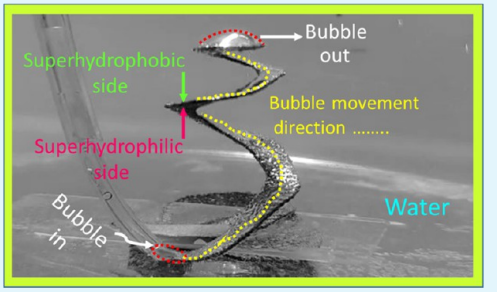

KEYWORDS: *Janus-faced carbon cloth, bubble transfer, poly(dimethylsiloxane) (PDMS), superaerophilic, superhydrophobic, superhydrophilic, gas bubble capture*

INTRODUCTION

Wettability at solid/liquid/gas interface, which is inspired by natural surfaces, has been widely studied and has many practical applications including anti-icing, oil−water separation, self-cleaning, fog harvesting, anticorrosion, microfluidics, etc.[1−3]

Janus materials with opposite wettability (superhydrophobicity and superhydrophilicity) have attracted a lot of attention. One of the most famous natural examples of Janus surfaces is the lotus leaf; its upper side is superhydrophobic (water contact angle > 150°) and oleophilic (oil contact angle < 90°), while the lower side is hydrophilic (water contact angle < 90°) and underwater oleophobic (oil contact angle > 90°).[4] Janus materials have a variety of practical applications, including fog harvesting,[5−8] membrane distillation,[9−11] humidity sensing,[12] directional liquid transfer,[13−15] solar desalination,[16−20] and oil−water separation,[21−24] and one of the applications that has recently been considered by researchers is the collection and transportation of gas bubbles.[25] The presence of bubbles in liquid systems is significant due to their application in various cases like wastewater treatment,[26] minerals recovery,[27] and solar energy harvesting. On the other hand, gas bubbles can have negative effects on pipes under certain conditions. Indeed, the presence of gas bubbles leads to an increase in the rate of corrosion and hydrogenation of the pipes. For example, hydrogen sulfide, carbon dioxide, and oxygen bubbles lead to corrosion of the pipes.[28,29] In recent years, controlled transportation of bubbles has become a very important challenge. Therefore, the attention of a number of researchers was oriented toward making samples that can transport and collect bubbles in a controlled fashion using elastic liquid infused materials,[30] superaerophilic geometry-gradient channels,[31] slippery liquid infused porous surfaces (SLIPSs),[32] Janus surfaces,[33] etc.

Underwater superaerophobic (bubble contact angle > 150°) or aerophobic (bubble contact angle > 90°) and superaerophilic (bubble contact angle < 10°)[1−3] surfaces have been applied to collect and transport subaqueous gas bubbles.[34,35] Superhydrophobic surfaces are underwater superaerophilic and superoleophilic, while superhydrophilic surfaces are underwater superaerophobic and superoleophobic.[36,37] Therefore, these surfaces possess bubble capture and antibubble proper-

Received: July 6, 2022
Accepted: September 12, 2022

https://doi.org/10.1021/acsami.2c12027
ACS Appl. Mater. Interfaces XXXX, XXX, XXX−XXX

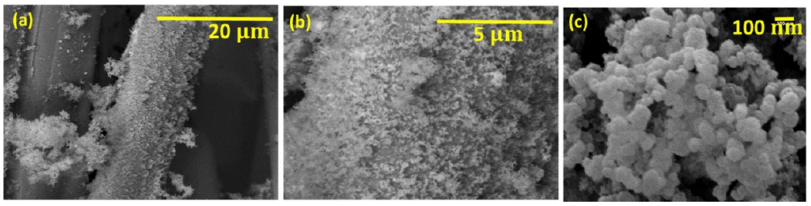

Figure 1. FE-SEM images at various magnifications of the flame-exposed side (superhydrophilic) of the Janus-CC.

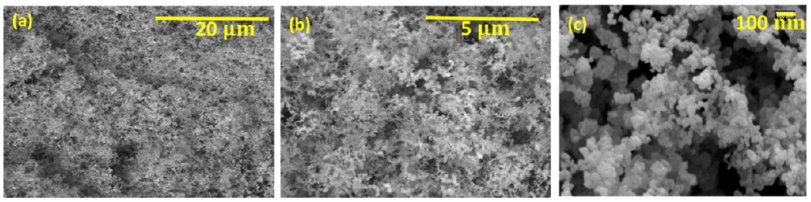

Figure 2. FE-SEM images at various magnifications of the side nonexposed to flame (superhydrophobic) of the Janus-CC.

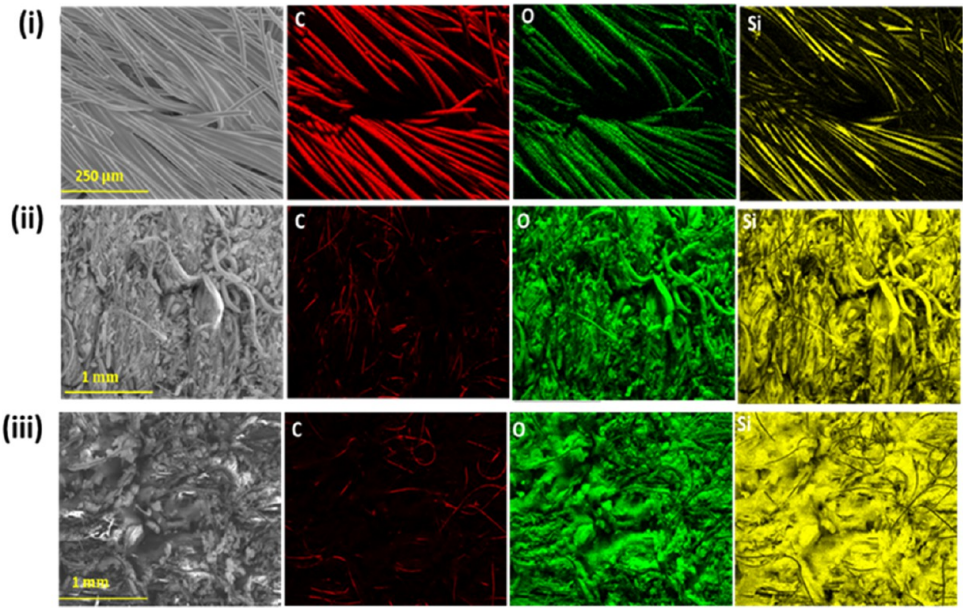

Figure 3. Element mapping images of (i) superhydrophobic carbon cloth, (ii) Janus-CC superhydrophilic side, and (iii) Janus-CC superhydrophobic side.

ties and could be applied to collect or repel bubbles, respectively.

Hu et al. synthesized a Janus membrane using a femtosecond laser-assisted ablation and nanoparticles deposition approach to achieve underwater unidirectional bubble infiltration.[38] Wang et al. prepared a Janus sample by spraying polydopamine on a polypropylene surface, and the synthesized sample was used for dye adsorption and bubble aeration.[39] Pei et al. designed a Janus mesh with the ability to unidirectionally transfer gas bubbles. The bubbles passed through the mesh from the superaerophobic side to the superaerophilic side underwater, but transportation in the opposite direction was not possible.[40] Chen and co-workers produced arrays of polydimethylsiloxane with the ability to control the bubble wettability gradient for underwater bubble unidirectional spontaneous transport.[41]

In recent years, the research activity in this field has been focused on the design of cost-effective, environmentally friendly, and low-energy methods for controlled transmission and removal of gas bubbles. Herein, a novel strategy was demonstrated for the preparation of Janus carbon cloth (Janus-CC) using PDMS coating and then burning one side of the sample on an alcohol burner. The prepared sample was characterized by different methods for its morphology, chemical composition, and wetting properties. The underwater bubble behavior on both sides of the Janus-CC was investigated, and the results showed that one side of the Janus-CC was superaerophilic, while the other side was aerophobic. The results obtained in this study hold great promise for designing cost-effective Janus materials for effective capture and controlled transportation of bubbles in fluids.

RESULTS AND DISSCUSSION

Characterization. The FE-SEM images in Figure S1, Supporting Information, revealed that the surface of the superhydrophobic PDMS-coated CC was smooth. The morphology of both sides of the CC changed dramatically after one side of the fabric CC was exposed to an alcohol f1f2

https://doi.org/10.1021/acsami.2c12027
ACS Appl. Mater. Interfaces XXXX, XXX, XXX−XXX

burner flame, Figures 1a−c and 2a−c. The appearance of nanoparticles on both sides of the sample was evident (size < 100 nm). It should be noted that the size of the nanoparticles on the face nonexposed to flame was smaller than that on the other side, i.e., flame-exposed face (Figures 1c and 2c). However, the deposited layer of nanoparticles on the side nonexposed to flame of the Janus-CC was much thicker than the flame-exposed side, which could be seen with the naked eye.

Figure S2a−c depicts the EDX elemental analysis results of the superhydrophobic PDMS-coated CC and both sides (superhydrophobic and superhydrophilic) of the Janus-CC. The EDX plot of the superhydrophobic CC contains C, O, and Si peaks, indicating the presence of a PDMS layer on the CC surface. The increased weight percentages of O and Si on both sides of the Janus-CC clearly reveal the formation of SiO_2 particles.

Elemental mapping images of the superhydrophobic and both sides of the Janus-CC are displayed in Figure 3i−iii. It could be clearly seen that C, O, and Si are uniformly distributed on all three surfaces. It is noteworthy that for the Janus-CC sample, the carbon abundance is lower but the O and Si contents are higher than for the superhydrophobic sample, confirming the formation of SiO_2 nanoparticles on both sides of the Janus-CC.

The ATR-IR spectra of both sides of the Janus-CC are depicted in Figure S3. For both sides of the sample, the broad peak at 1080−1090 cm^{-1} is assigned to the Si−O−Si bond stretching of SiO_2 due to the formation of SiO_2 nanoparticles on both sides of the Janus-CC. For the superhydrophobic side, a peak at 803 cm^{-1}, which belongs to the $Si-CH_3$ bending, is observed, indicating the presence of PDMS and its oligomers.[42−44]

To identify the elements on the surface and their chemical environment, XPS analysis was performed on pristine CC, superhydrophobic CC (PDMS-coated CC), and both sides of the Janus-CC samples. The survey spectrum of pristine CC is shown in Figure S4a. It comprises two peaks at 285.0 and 532.0 eV corresponding to C 1s and O 1s, respectively. As determined from this spectrum, about 95% of the CC surface is composed of carbon atoms. The high-resolution XPS spectrum of the C 1s is depicted in Figure S4b. The fitting results reveal that the mentioned peak consists of three bands: the most intense peak at 285.0 eV belongs to carbon−carbon (C−C) or hydrogen (C−H) bonds, the band at 286.0 eV is due to C−O, and the peak at 290.2 eV is ascribed to COO groups. Therefore, it can be concluded that the pristine carbon cloth surface mainly comprises carbon, along with a small amount of oxygen-containing functional groups, originating from surface contamination or slight oxidation of the CC surface during storage and handling. Figure S5a exhibits the survey XPS spectrum of the superhydrophobic (PDMS-coated) CC. It consists of three elements: Si 2p (103.1 eV), C 1s (285.0 eV), and O 1s (532.0 eV) with different atomic percentages; the percentage of oxygen on the surface of this sample is high, which is related to the PDMS coating. The high-resolution XPS spectrum of C 1s (Figure S5b) could be fitted with the main component at 285.0 eV corresponding to C−C/C−H bonds. The Si 2p band (Figure S5c) comprises a main component at 103.1 eV assigned to silicon bonded to oxygen ($Si-O_x$), confirming the presence of PDMS on the surface of this sample. For the superhydrophilic side of the Janus-CC, the wide XPS spectrum in Figure 4a reveals three peaks at 285.0,

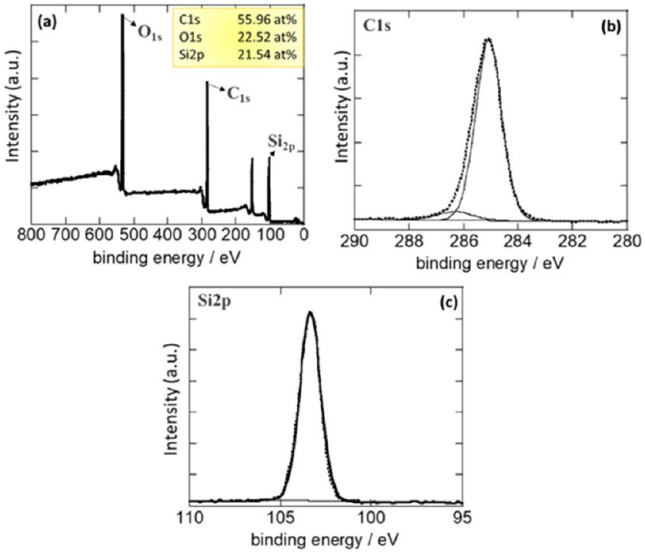

Figure 4. (a) XPS survey spectrum and high-resolution spectra of (b) C 1s and (c) Si 2p of the superhydrophilic side of the Janus-CC sample.

103.1, and 532.0 eV ascribed to C 1s, Si 2p, and O 1s, respectively. Figure 4b displays the high-resolution spectrum of the C 1s. It could be curve-fitted with two peaks at 285.0 eV (C−C/C−H) and 286.0 eV (C−O). Figure 4c depicts the high-resolution spectrum of Si 2p, which consists of only one peak at 103.5 eV due to SiO_2. The results infer that the superhydrophilic side of the Janus-CC sample is essentially composed of SiO_2 and carbon. Figure 5a exhibits the survey

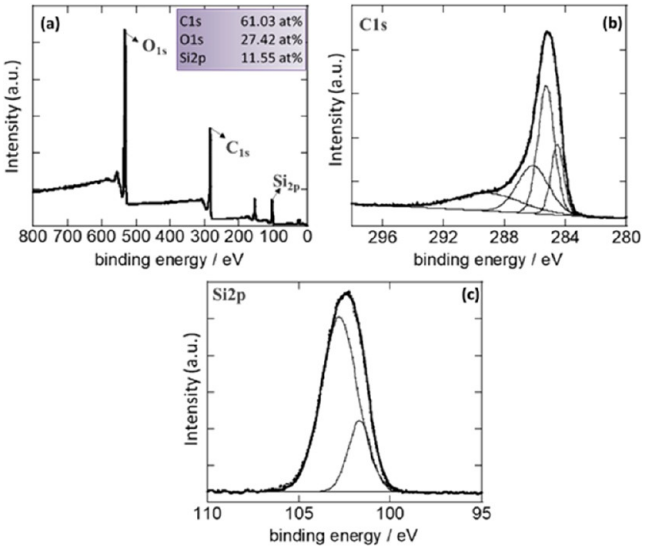

Figure 5. (a) XPS survey spectrum and high-resolution spectra of (b) C 1s and (c) Si 2p of the superhydrophobic side of the Janus-CC sample.

XPS spectrum of the superhydrophobic side of the Janus-CC sample. It features similar peaks at 103.1, 285.0, and 532.0 eV ascribed respectively to Si 2p, C 1s, and O 1s. The high-resolution spectrum of C 1s (Figure 5b) could be deconvoluted into several bands at 284.5 eV (Si−C), 285.5 eV (C−C/C−H), 286.5 eV (C−O), and 289.1 eV (COO). These peaks originate from PDMS and its oligomers on the

https://doi.org/10.1021/acsami.2c12027
ACS Appl. Mater. Interfaces XXXX, XXX, XXX−XXX

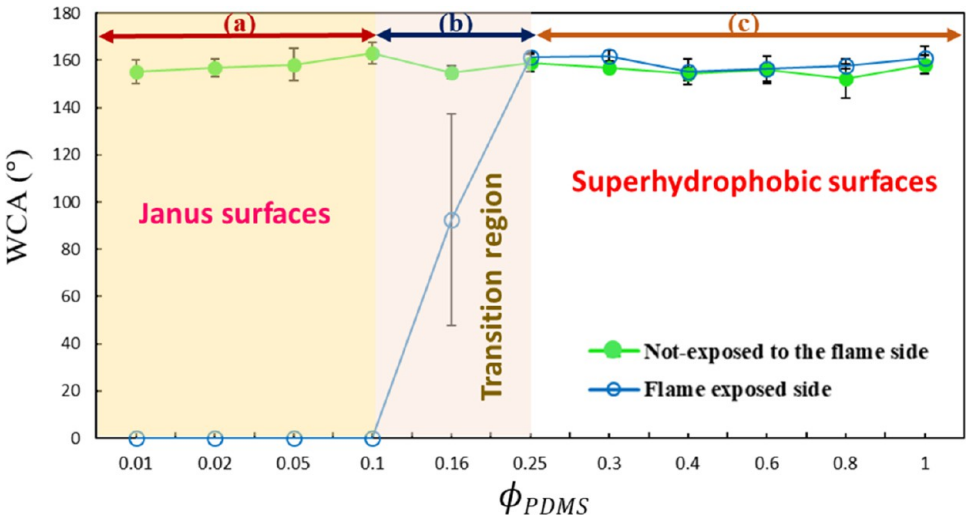

Figure 6. Diagram of WCA changes on both sides of the prepared Janus-CC samples as a function of ϕ_{PDMS}.

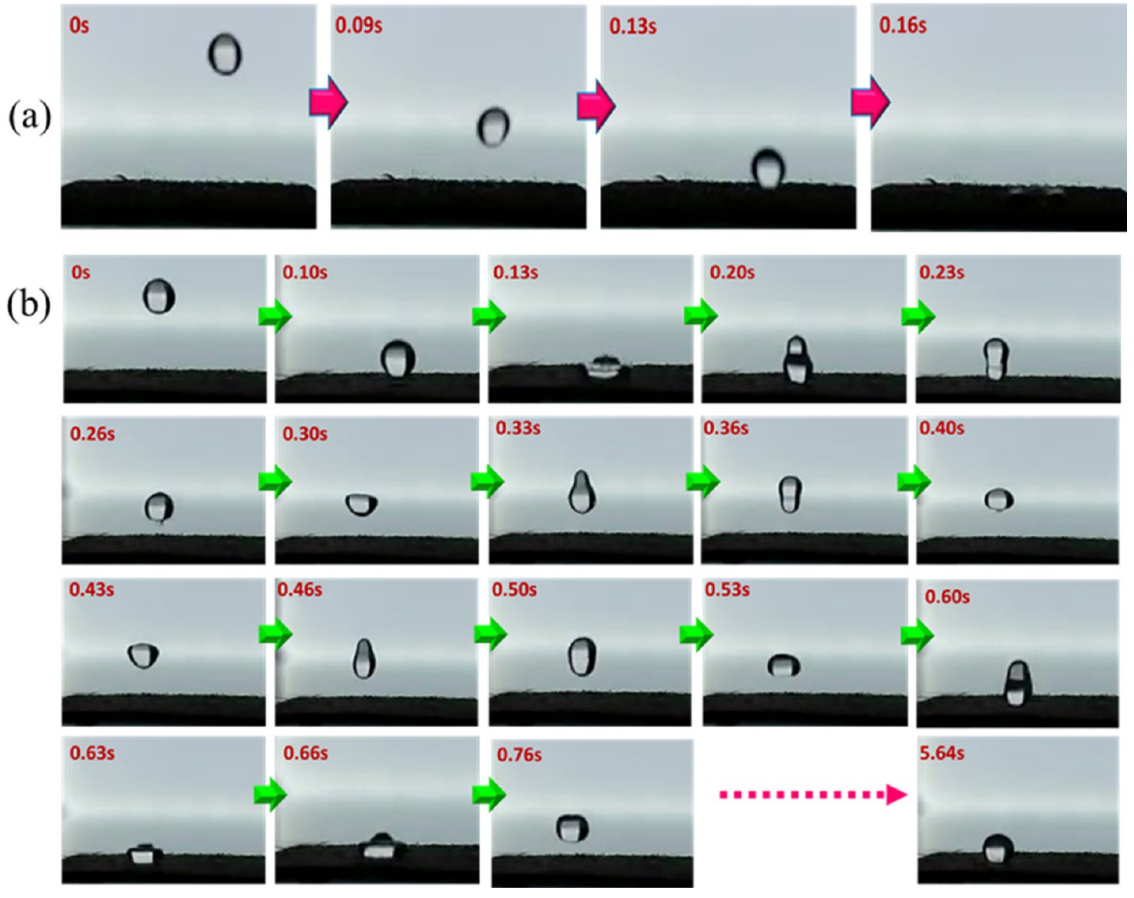

Figure 7. Sequential images of the impact of a falling water droplet on the (a) superhydrophilic and (b) superhydrophobic sides of the Janus-CC sample.

superhydrophobic side of the Janus-CC. The high-resolution spectrum of Si 2p (Figure 5c) could be fitted with two peaks at 102.1 and 103.6 eV related to PDMS and SiO_2, respectively.[42] Therefore, the presence of SiO_2 nanoparticles adhering to the carbon surface on the superhydrophobic side of the Janus-CC sample is clearly confirmed. ~~Therefore~~, based on all of the studied characterization methods, it can be concluded that the superhydrophilic side of the Janus sample consists of SiO_2 nanoparticles deposited on carbon cloth, whereas the superhydrophobic side comprises a very thin layer of PDMS and its oligomers coated on the surface of SiO_2 nanoparticles deposited on the carbon cloth.

Based on the obtained analysis results, the proposed structure of the prepared Janus-CC is schematically presented in Figure S6b.

The effect of different amounts of PDMS on the wetting properties of both sides (exposed and nonexposed to the flame) of the synthesized sample was investigated through

https://doi.org/10.1021/acsami.2c12027
ACS Appl. Mater. Interfaces XXXX, XXX, XXX−XXX

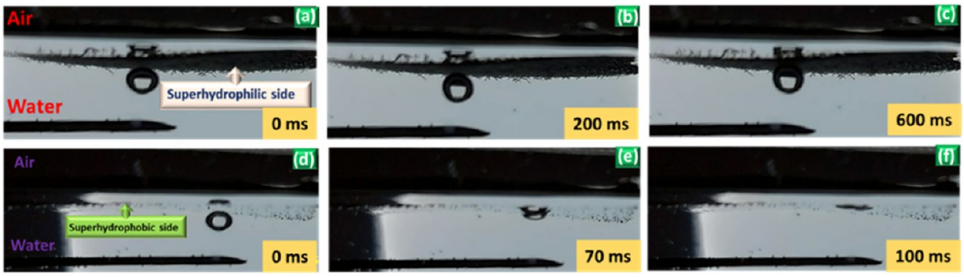

Figure 8. Bubble behavior at the air−water interface of the (a−c) superhydrophilic and (d−f) superhydrophobic sides in contact with water.

water contact angle (WCA) and sliding angle (SA) measurements. Figure 6 presents the diagram of the measured WCA versus ϕ_{PDMS}, which can be divided into three separate sections. In region "a" ($0.01 \leq \phi_{PDMS} \leq 0.1$), the prepared samples are Janus; thus, the flame-exposed side is superhydrophilic and the side nonexposed to flame is superhydrophobic. In region "b" ($0.1 < \phi_{PDMS} \leq 0.25$), the WCA of the flame-exposed side changes from 0 to 155°; therefore, the wettability of this side changes from superhydrophilic to superhydrophobic, while the WCA of the other side remains high and constant (~155°; superhydrophobic). In region "c" ($0.25 < \phi_{PDMS} \leq 1$), the synthesized samples are completely superhydrophobic. Figure S7 shows the sliding angle on the surface of the synthesized samples. At $0.01 \leq \phi_{PDMS} \leq 0.1$, the flame-exposed side has a superhydrophilic property and is wetted completely by water. However, at $\phi_{PDMS} > 0.2$, the SA is lower than 2°. For the side nonexposed to flame, the sliding angle decreases from 5° ($\phi_{PDMS} = 0.01$) to 2° ($0.05 \leq \phi_{PDMS}$). According to the results of Figures 6 and S7, $\phi_{PDMS} = 0.1$ was selected for the fabrication of the Janus-CC.

It has been previously reported that the thermal decomposition of PDMS, in air, leads to the formation of a mixture of oligomers, carbon dioxide, and a very soft powder of SiO_2.[42] Therefore, it could be concluded that when the PDMS-coated CC was exposed to an alcohol lamp flame, a small amount of SiO_2 was formed on the higher-temperature side, which leads to surface superhydrophilicity. However, a large amount of SiO_2 is also formed on the backside (PDMS-coated CC nonexposed to flame) of the CC, which is the reason for the whitening of the surface (Figure S6). On the side nonexposed to flame of the CC, the deposition of SiO_2 nanoparticles led to an increase of surface roughness. The enhanced roughness combined with the adsorption of evaporated PDMS and its oligomers on the surface of SiO_2 nanoparticles confers a superhydrophobic character to the side nonexposed to flame of the CC. Therefore, a Janus-CC featuring both superhydrophilic and superhydrophobic sides is formed easily.

To evaluate the stability of the wettability of both sides of the Janus-CC, WCA measurements at different time intervals were performed (Figure S8). Also, the water sliding angle was assessed at different time intervals, and no change was observed over a long period. Therefore, the wettability properties of the synthesized Janus-CC are stable for a long time (53 days).

Investigation of Thermal Stability. The thermal stability of the prepared Janus-CC was examined by heating in an electric furnace (Figure S9). The furnace temperature reached 100 °C at a speed of 10 °C/min and was kept at this temperature for 1 h; then, the temperature reached the desired temperature (200, 300, 400, and 500 °C) and was maintained for 4 h. The WCA, measured on the superhydrophobic side of the Janus-CC, was stable up to 400 °C. However, at higher temperatures, because of the desorption and decomposition of adsorbed PDMS and its oligomers, the surface lost its hydrophobicity and became superhydrophilic.

Falling Droplets on the Superhydrophilic and Superhydrophobic Surfaces of the Janus-CC. In this section, a water droplet was dropped on both sides of the Janus sample and the images were recorded with a slow-motion camera. The water droplet spreads quickly on the superhydrophilic side of the Janus-CC (less than 0.1 s) (Figure 7a). On the superhydrophobic side of the Janus-CC, the falling water droplet impacts the surface, slightly spreads, then shrinks, bounces several times, and finally rests on the surface with a spherical shape (Figure 7b). This behavior is characteristic of a superhydrophobic surface.[46−48]

Determination of Surface Energy of Janus-CC. Figure S10 depicts the Zisman diagram for the determination of the surface energy of the superhydrophobic side of the Janus-CC. The obtained critical surface tension for the superhydrophobic side is about 40.7 mN/m. So, any organic solvent with $\gamma \leq 40.7$ mN/m can wet the superhydrophobic side of the Janus-CC.

Wettability of the Janus-CC at Different Interfaces. The wettability of the Janus-CC at the oil−water and air−water interfaces was investigated. Figure S11a shows a Janus-CC at the oil−water interface; the sample is placed in such a way that the superhydrophobic side is in contact with oil and the superhydrophilic side is in contact with water. As seen in the figure, despite the contact of the superhydrophobic surface with oil, the sample still retains its superhydrophobicity and is stable at the two-phase interface. On the other hand, a Janus-CC was placed in the opposite direction at the oil−water interface (Figure S11b) and water droplets were injected into the superhydrophilic side; the surface is still superhydrophilic and is wetted completely. The injection of water droplets continued until the surface became saturated, and then the collected water drained to the aqueous phase.

In another experiment, Janus-CC was placed at the air−water interface and the oil wettability was evaluated on both sides of the Janus sample. In Figure S12a, the superhydrophobic side of the Janus-CC was in contact with water and then an oil droplet was injected into the surface. It was seen that the oil droplet rapidly absorbs and spreads on the superhydrophobic side of the Janus-CC surface, indicating its oleophilicity. Then, the sample was inverted such that the superhydrophilic side was in contact with the water (Figure S12b). When an oil droplet was injected, it maintained its spherical shape, confirming its oleophobicity. To further evaluate the performance of the Janus-CC, it was completely immersed in a water container and oil was injected into both sides. It is obvious that the superhydrophilic side of the Janus-CC is oil-repellent underwater and the oil droplet remains

https://doi.org/10.1021/acsami.2c12027
ACS Appl. Mater. Interfaces XXXX, XXX, XXX−XXX

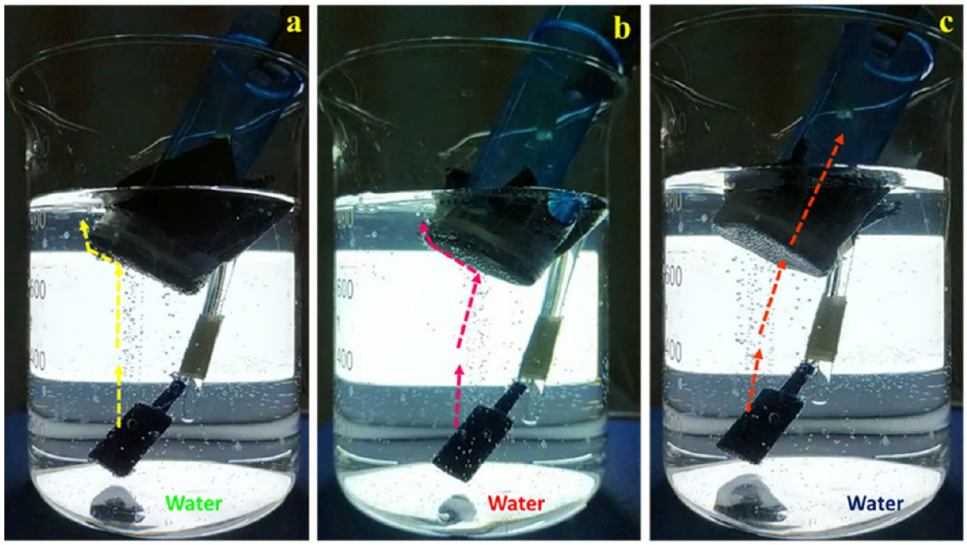

Figure 9. Continuous flow of tiny gas bubbles hitting (a) pristine carbon cloth, (b) superhydrophilic side of the Janus-CC, and (c) superhydrophobic side of the Janus-CC.

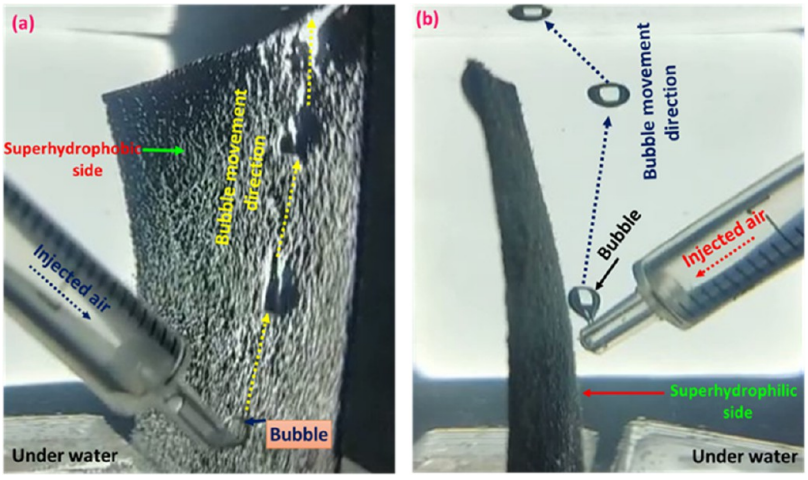

Figure 10. Injection of bubbles into the vertically positioned Janus-CC: (a) superhydrophobic side, and (b) superhydrophilic side.

spherical (Figure S13a). For the superhydrophobic side of the Janus-CC, the oil droplets spread immediately and the surface exhibits underwater oleophilicity (Figure S13b, Supporting Information). Figure S14 illustrates the lotus leaf property of the prepared Janus-CC, which floats stably at the air−water interface in such a way that the upper side is superhydrophobic and the bottom side is superhydrophilic and also underwater oleophobic.

Gas Bubble Behavior of the Janus-CC Positioned at the Air−Water Interface. The aerophilicity of the prepared Janus-CC was investigated by placing it at the air−water interface and then injecting a bubble. As shown in Figure 8a−c, when the superhydrophilic side is in contact with water, the bubble cannot pass through the Janus-CC because the superhydrophilic side is completely wetted and covered with water, creating a polar surface, which repels the bubble (nonpolar medium). On the other hand, when the superhydrophobic side is in contact with water, the bubble passes easily through the Janus-CC membrane within 100 ms (Figure 8d−f). In this case, the surface is not wetted by water and retains its nonpolar character and also porosity and hence attracts the bubble.

Underwater Collection of a Continuous Flow of Gas Bubbles. According to the behavior of the synthesized sample in dealing with bubbles, an experiment was designed using a continuous flow of tiny bubbles in such a way that a tube was covered with pristine CC or the superhydrophobic or superhydrophilic side of the Janus-CC, Figure 9. When the tiny gas bubbles hit the surface of pristine CC and superhydrophilic side of the Janus-CC, their direction changes and they move toward the surface of water, Figure 9a,b. In contrast, when the flow of the tiny gas bubbles hits the superhydrophobic side of the Janus-CC, the bubbles are absorbed by the surface and transferred into the tube, Figure 9c. This interesting behavior of the Janus-CC suggests that it can be used for the collection of gas bubbles released in aqueous media.

Injecting Gas Bubbles into the Vertically Aligned Janus-CC Immersed in Water. In this part, a Janus-CC was immersed vertically in a water container; then, gas bubbles were injected into both sides of the Janus-CC surface using a syringe. Interestingly, the superhydrophilic side repels the bubbles, while the superhydrophobic side captures all of the

https://doi.org/10.1021/acsami.2c12027
ACS Appl. Mater. Interfaces XXXX, XXX, XXX−XXX

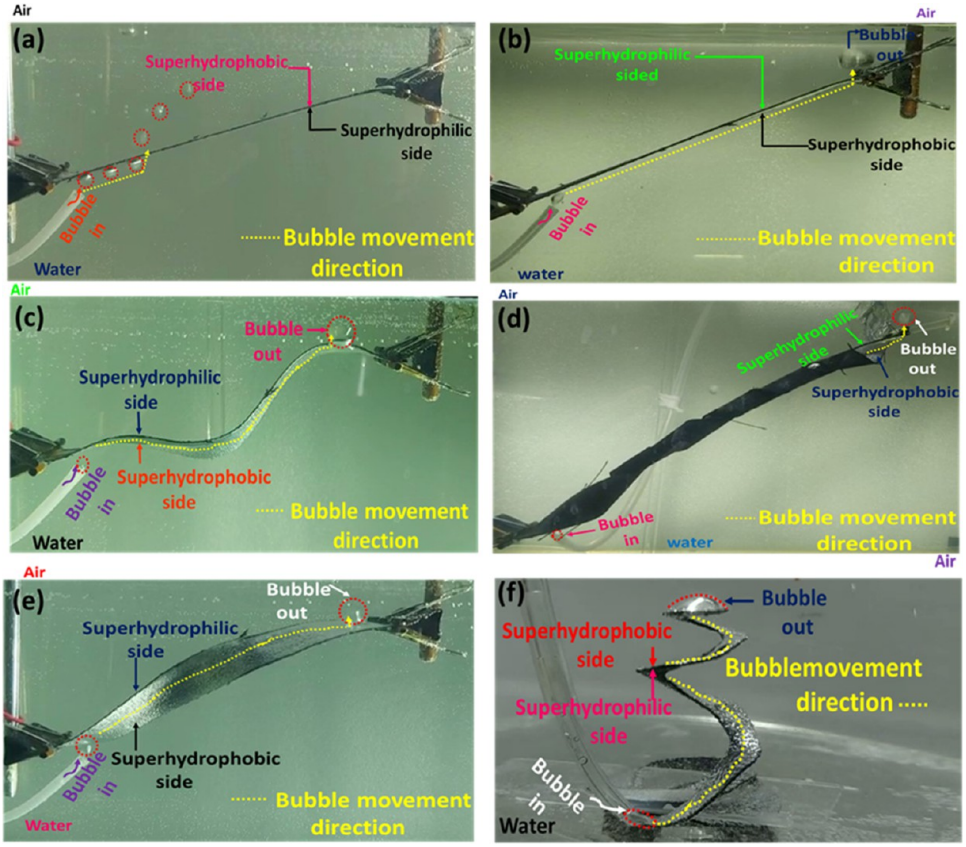

Figure 11. Bubble capture and transportation by the superhydrophobic side of the Janus-CC strip with different shapes. (a) Inclined shape with the superhydrophobic side at the bottom, (b) inclined shape with the superhydrophobic side at the bottom, (c) curved shape, (d) twisted with a high degree of torsion, (e) twisted with a low degree of torsion, and (f) spiral shape.

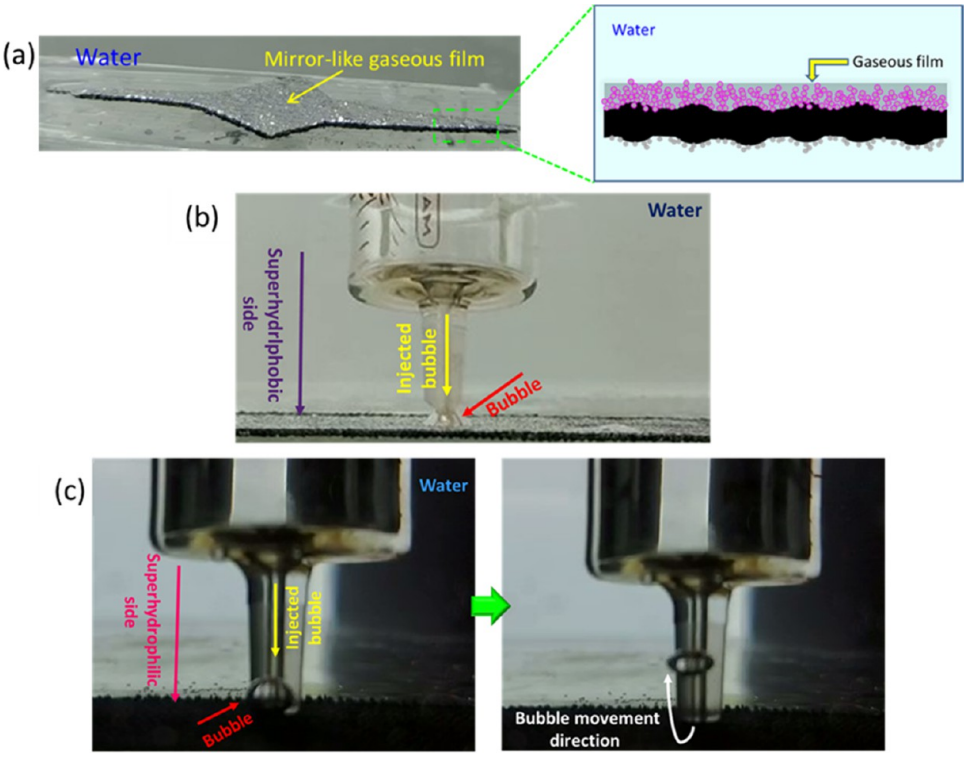

Figure 12. (a) Formation of a mirrorlike gaseous film on the superhydrophobic side of the Janus-CC immersed into water and underwater injection of a gas bubble into the (b) superhydrophobic and (c) the superhydrophilic sides of the Janus-CC.

https://doi.org/10.1021/acsami.2c12027
ACS Appl. Mater. Interfaces XXXX, XXX, XXX−XXX

injected bubbles and transfers them into the collecting tube (Figure 10 and Video S1).

Gas Bubble Absorption and Transportation. In this section, the performance of the Janus-CC in bubble transportation was further assessed. Initially, a long strip of Janus-CC was made and positioned in an inclined orientation. When the air pump is turned on, the gas bubbles leave the superhydrophilic side after a short distance and enter the bulk water, Figure 11a. For the reverse position, the superhydrophobic surface acts as a bridge, directing the incoming bubbles to the end of the strip, Figure 11b. To evaluate and demonstrate the ability of the Janus-CC strip for bubble transportation, the Janus strip was reformed into various shapes, including curved (Figure 11c), completely twisted (Figure 11d), partially twisted (Figure 11e), and spiral (Figure 11f). The results of the experiments clearly evidenced that, under any torsional conditions, the superhydrophobic side of the Janus strip is capable of targeted bubble transfer. Figure S15 depicts a close-up view of bubble transfer on the superhydrophobic side of the twisted Janus-CC strip with a low torsional degree. Also, Video S2 shows the excellent performance of the spiral Janus-CC strip for capturing and transporting gas bubbles.

To further test the ability of the superhydrophobic side of the Janus-CC to transfer bubbles, a thin strip of the sample was placed in a water container. The bottom part of the sample was positioned next to the bubble production tube, and its upper part was placed inside an inverted cylindrical glass containing colored water (Figure S16). As can be seen, the superhydrophobic surface of the Janus-CC acts as a bridge for the targeted transport of bubbles, and the reduction in the height of the colored water column clearly indicates the ability of the sample to transport bubbles.

The bubble transfer rate on an inclined Janus-CC strip was investigated at various tilting angles (α). The results in Figure S17 reveal that, by increasing α, the bubble transfer rate increases. It is worth noting that at very low angles (10°), the transfer rate is also high (rate > 16 cm/s).

The Janus-CC was attached to a glass slide surface and placed horizontally at the bottom of a water container. As shown in Figure 12a, the superhydrophobic side of Janus-CC exhibits a mirrorlike feature underwater due to the formation of a gaseous film on its surface. Since the superhydrophobic side is completely nonpolar and porous, air (as a nonpolar phase) is trapped inside it, and by placing the sample underwater, a gaseous film is formed at the solid−liquid interface, Figure 12a. This gaseous film is very stable, and when a bubble is injected into the superhydrophobic side, the bubble is tethered to the surface due to the cohesion force between the gas bubble and the gaseous film, Figure 12b. Therefore, underwater, the superhydrophobic side of Janus-CC is superaerophilic, but when the bubble is injected into the superhydrophilic side of the Janus-CC, the bubble is repelled, Figure 12c, because the superhydrophilic side is completely covered by water and forms a polar medium and therefore is superaerophobic.

Since the superhydrophobic side of the Janus-CC displays underwater superaerophilic character, more detailed studies were performed. Figure 13 and Video S3 exhibit interesting behavior of the superhydrophobic side underwater. First, a bubble was injected into the surface, the bubble was absorbed and stayed on the surface in the form of a paraboloid of revolution shape (Figure 13a). Then, a smaller bubble was

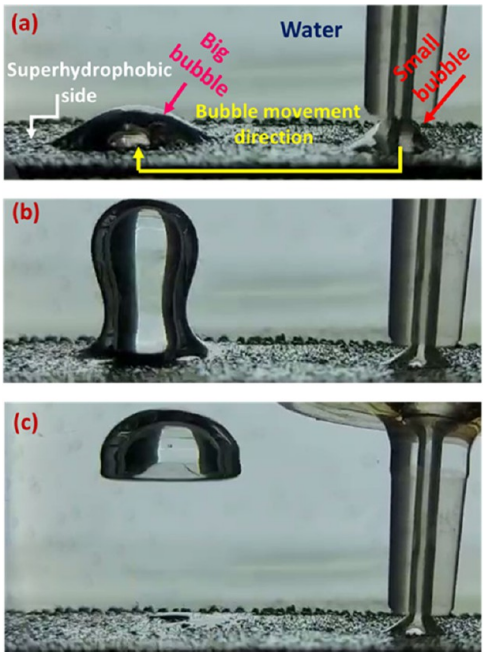

Figure 13. Transfer of a small bubble toward a larger one on the superaerophilic surface via the gaseous film.

injected into another place on the surface, Figure 13b. The small bubble was absorbed and migrated through the gaseous film toward the larger bubble and then merged into a bigger one. The reason for the migration of the smaller bubble to the larger one is the difference in Laplace pressure. Finally, they merge and a big bubble detaches from the surface due to the buoyant force, Figure 13c and Video S3.

For a better understanding of the mechanism of bubble transfer on the superhydrophobic surface of the Janus-CC sample through the gaseous film, various designs of the Janus-CC were made and the bubble transfer abilities were investigated. In all designed patterns (flowerlike, triangular, etc.), the Janus sample has both narrow and wide parts (Figure 14). In all tested designs, it was observed that if the bubble was injected into the narrow part of the sample, it spontaneously and quickly transferred to the wider part through the gaseous film, whereas if the bubble was injected into the wide part of the sample, it was tethered and remained there in the form of a paraboloid of revolution shape. The reason for the spontaneous transfer of the bubble from the narrow to the wide part of the sample is due to the presence of higher structural Laplace pressure in the narrow part of the sample,[45] which causes the bubble to be transferred to the part with a lower structural Laplace pressure (wide part of the sample). For the flowerlike structure, it was seen that, by injecting the bubbles into the center of the sample (narrow part of the sample), the bubbles were distributed spontaneously and rapidly toward all petals (wide part of the sample). This interesting result indicates that the Janus-CC with the flowerlike pattern can be used for bubble distribution and transfer to different places, Figure 14 and Video S4.

In another experiment, the bubble transfer process on the superaerophilic side of an inclined Janus-CC (α = 30°) with a rectangular shape (having no structural Laplace pressure) was examined (Video S5). At an angle of 30° when the bubble was injected into the lower part of the sample, it was transmitted through the gaseous film and finally exited from the upper part

https://doi.org/10.1021/acsami.2c12027
ACS Appl. Mater. Interfaces XXXX, XXX, XXX−XXX

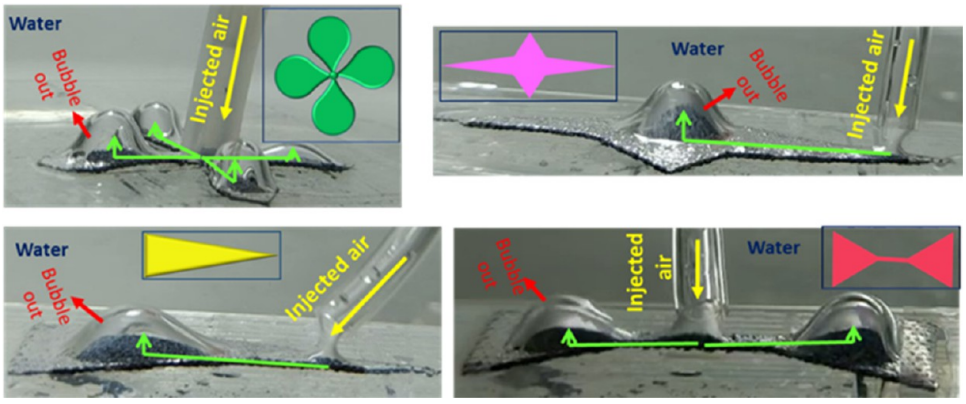

Figure 14. Movement of bubbles on the superaerophilic side of the Janus-CC from the narrow to wide part.

of the sample due to the buoyant force, Figure 15a. In the next experiment, the Janus-CC with a triangular shape was placed in

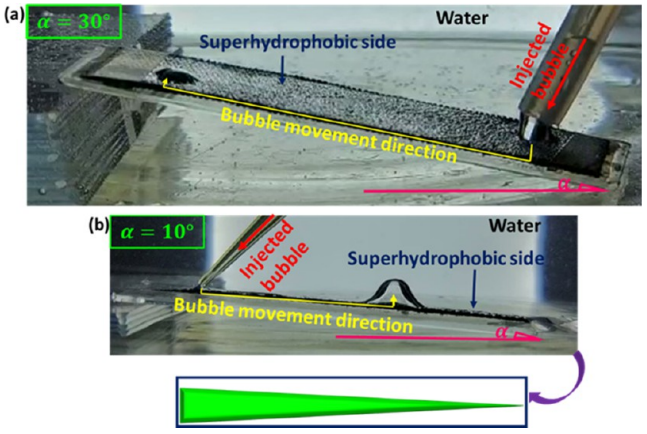

Figure 15. Bubble transfer on the superaerophilic side of an inclined Janus-CC: (a) on a rectangular sample and the movement is in the direction of the buoyant force and (b) on a triangular sample and the movement is in the opposite direction of the buoyant force.

an inclined position at an angle of 10° so that the vertex of the triangle points upward and its base faces downward. The bubble was injected into the vertex of the triangle, and surprisingly, it was observed that the bubble moved downward and exited from the bottom side near the triangle base, Figure 15b. The reason for this downward movement is the dominance of structural Laplace pressure of the narrow part of the surface over the buoyant force.

To evaluate the bubble transfer performance of the Janus-CC at high temperatures, the bubble movement in boiling water in the absence and presence of Janus-CC was investigated (Figure S18). The result revealed that the superaerophilic side of the Janus-CC captures the released bubbles and increases their upward movement. The obtained rate of bubble movement in bulk water is 0.05 m/s, while for Janus-CC, it is 0.31 m/s.

In the next part, an experiment was designed to evaluate the ability of the Janus-CC to transport bubbles under harsh physical conditions. In this experiment, air was pumped from the bottom side of a container of water and sand (Figure S19a). In the absence of the Janus-CC sample, the bubbles came out irregularly from different positions on the sand surface (Figure S19a). In contrast, when a Janus strip was placed inside the water/sand container, all of the bubbles were captured by the superaerophilic side of the Janus-CC and transferred to the surface of the water in one direction (Figure S19b). As a result, the Janus-CC has retained its ability to transport bubbles under harsh physical conditions, and it can be used for gas bubble transport even inside the sand.

Applications of the Janus-CC for Gas Bubble Transfer. *Unidirectional Gas Membrane.* A setup was designed to assess the gas transfer into the liquid phase through a Janus-CC membrane. A Janus-CC piece was placed between two tubes as a membrane in a way that the superhydrophobic side was in the upward direction (in contact with the aqueous phase) and the superhydrophilic side was in the downward direction. In the next step, an alkaline solution of phenolphthalein was poured into the upper tube. The remarkable point is that, due to the superhydrophobicity of the upper side, the solution could not move downward and remained on the membrane. The lower tube was connected to a CO_2 source. It was obvious that the CO_2 gas was easily transferred from the superhydrophilic to the superhydrophobic side. With the entry of CO_2 gas bubbles into the alkaline solution of phenolphthalein, the pH of the solution decreased ($2NaOH + CO_2 \rightarrow Na_2CO_3 + H_2O$) and the color of the solution changed from pink to colorless within 49 s (Figure S20 and Video S5). So, the Janus-CC did not permit the aqueous solution to move downward, while allowing the gas to pass through it in the upward direction. The results clearly indicate that the Janus-CC could be successfully applied as a membrane (or valve) for gas entering into an aqueous solution.

Underwater Gas Transformation for Reaction. Simultaneous underwater transfer of CH_4 and air was examined by a Janus-CC. Two Janus strips were placed at the bottom of a water container in a way that the upper parts of the two carbon strips were put inside a glass syringe. Then, air was injected into the bottom part of one of the Janus strips and methane gas into the other one. It follows that CH_4 and air were transported into the glass syringe by the Janus strips and mixed with each other, confirmed using a flame at the tip of the syringe (Figure S21).

Debubbling in the Fluid Transfer Pipe. An experiment was performed to demonstrate the effective role of Janus-CC in debubbling in a fluid transfer pipe (Figure S22). Water stream and air were injected into a pipe having a duct for bubble exit; both bubbles and water droplets exited from the duct (Figure S22a). Upon placing a piece of a Janus-CC in the duct in such a way that the superhydrophobic (superaerophilic) side becomes the outer side, the moving bubbles were strongly

https://doi.org/10.1021/acsami.2c12027
ACS Appl. Mater. Interfaces XXXX, XXX, XXX−XXX

captured by the Janus-CC, but the water was repelled, and only bubbles could exit from the duct (Figure S22b). This experiment evidences the ability of Janus-CC to debubble from the liquid stream in a pipe and prevent the secondary problems caused by bubbles (such as corrosion of pipes).

CONCLUSIONS

In this paper, Janus-faced carbon cloth (Janus-CC) was successfully fabricated by a novel, cost-effective, fast, and simple strategy. The hydrophilic side of the sample was composed of a thin layer of deposited SiO_2 nanoparticles, while its superhydrophobic side consisted of a thick layer of SiO_2@PDMS. The superhydrophobic face of the Janus-CC displayed a superaerophilic property underwater. Thanks to the superaerophilic character, the Janus-CC demonstrated the ability to spontaneously capture and directionally transport underwater gas bubbles. The Janus-CC with a strip shape was able to transfer gas bubbles at a long distance with a high speed at any torsional degree. The underwater gaseous film formed on the superaerophilic side of the Janus-CC was responsible for its successful capture and transport of the bubbles. Our Janus-CC was not only capable of the collection and controlled transfer of bubbles but also featured the ability of unidirectional penetration of underwater gas. The prepared Janus-CC had high thermal, mechanical, and long-life stability. The presented strategy and material provided new insights into the fabrication of advanced surfaces with high performance for fast capture, collection, and targeted transfer of underwater bubbles. The prepared Janus-CC was successfully utilized as a controlled underwater gas bubble transporter, a membrane for unidirectional gas permeation and reaction in the aqueous phase, an underwater gas transporter for reaction, and material for debubbling of a fluid stream in a pipe.

EXPERIMENTAL SECTION

Materials. Carbon cloth (CH-900−15) with a thickness of 0.50 ± 0.05 mm was purchased from Kuraray Chemical Co., Ltd., Japan. Polydimethylsiloxane (PDMS, Sera Sense SF 350 Korea) and *n*-hexane (≥95%, Merck Co.) were used as received.

Preparation of Janus-Faced Carbon Cloth (Janus-CC). The process of Janus carbon cloth (Janus-CC) preparation is schematically presented in Figure S20. The carbon cloth (CC) pieces were immersed in a binary mixture of PDMS and *n*-hexane at different volume fractions of PDMS (ϕ_{PDMS} = 0.01, 0.02, 0.05, 0.1, 0.25, 0.4, 0.6, 0.8, and 1) for 30 s. Then, the CC samples were left at room temperature for 1 day for slow *n*-hexane evaporation. The obtained CC at this stage was superhydrophobic.[49] Finally, one side of the dried sample was placed on top of an alcohol burner flame for 60 or 90 s. At this stage, the flame (~500 °C)-exposed side of the PDMS-modified CC lost its PDMS coating by evaporation and decomposition and became superhydrophilic. On the other hand, the other side of the CC (nonexposed to the flame) remained superhydrophobic because of the deposition of the decomposed and evaporated products of PDMS from the other side. Therefore, by this novel and simple method, a Janus-CC was obtained (Figure S23).

ASSOCIATED CONTENT

Supporting Information

The Supporting Information is available free of charge at https://pubs.acs.org/doi/10.1021/acsami.2c12027.

FE-SEM images of the superhydrophobic carbon cloth, EDX spectra of superhydrophobic carbon cloth and Janus-CC samples, ATR-IR spectra of the Janus-CC sample, XPS survey spectra of samples, schematic of the structure of Janus carbon cloth, sliding angle of the water droplet on both sides of the Janus-CC, water contact angles at different time intervals, stability of Janus-CC, Zisman diagram of the Janus-CC, wettability of the Janus-CC at the air−water and kerosene-water interfaces, underwater oleophobic/oleophilic properties of the Janus-CC, lotus leaf behavior of the Janus-CC, bubble transfer route on the Janus-CC twisted strip, bubble movement rate diagram, images of bubble movement at boiling temperature, movement path of gas bubbles in sand−water, unidirectional gas membrane, simultaneous underwater transfer of two gases by two Janus ~~carbon cloth,~~ water and bubble flow in a pipe, and scheme of Janus ~~carbon cloth~~ preparation method (PDF)

Superhydrophilic side repelling the bubbles, while the superhydrophobic side capturing all of the injected bubbles and transferring them into the collecting tube (AVI)

Excellent performance of the spiral Janus-CC strip for capturing and transporting gas bubbles (AVI)

Interesting behavior of the superhydrophobic side underwater (AVI)

Janus-CC with the flowerlike pattern used for bubble distribution and transfer to different places (AVI)

Bubble transfer process on the superaerophilic side of inclined Janus-CC (α = 30°) with a rectangular shape (AVI)

Video S6 (AVI)

AUTHOR INFORMATION

Corresponding Author

Saeid Azizian − *Department of Physical Chemistry, Faculty of Chemistry, Bu-Ali Sina University, 65167 Hamedan, Iran;* orcid.org/0000-0003-0040-3478; Email: sazizian@basu.ac.ir

Authors

Haniyeh Tahzibi − *Department of Physical Chemistry, Faculty of Chemistry, Bu-Ali Sina University, 65167 Hamedan, Iran*

Sabine Szunerits − ~~*Universite*~~ *Lille, CNRS, Centrale Lille,* ~~*Universite*~~ *Polytechnique Hauts-de-France, UMR 8520, IEMN, F-59000 Lille, France;* orcid.org/0000-0002-1567-4943

Rabah Boukherroub − *Universite Lille, CNRS, Centrale Lille,* ~~*Universite*~~ *Polytechnique Hauts-de-France, UMR 8520, IEMN, F-59000 Lille, France*

Complete contact information is available at: https://pubs.acs.org/10.1021/acsami.2c12027

Author Contributions

The manuscript was written through the contribution of all authors. All authors have given approval to the final version of the manuscript.

Funding

The authors acknowledge the financial support from Bu-Ali Sina University (Grant Number: 99-242).

Notes

The authors declare no competing financial interest.

■ ACKNOWLEDGMENTS

Donation of carbon cloth by Professor M. Aratono (Kyushu University) is highly appreciated.

■ REFERENCES

(1) George, J. E.; Chidangil, S.; George, S. D. Recent Progress in Fabricating Superaerophobic and Superaerophilic Surfaces. *Adv. Mater. Interfaces* **2017**, *4*, No. 1601088.

(2) Yong, J.; Chen, F.; Li, M.; Yang, Q.; Fang, Y.; Huo, J.; Hou, X. Remarkably Simple Achievement of Superhydrophobicity, Superhydrophilicity, Underwater Superoleophobicity, Underwater Superoleophilicity, Underwater Superaerophobicity, and Underwater Superaerophilicity on Femtosecond Laser Ablated PDMS Surfaces. *J. Mater. Chem.* **2017**, *5*, 25249−25257.

(3) Latthe, S. S.; Sutar, R. S.; Bhosale, A. K.; Nagappan, S.; Ha, C. S.; Sadasivuni, K. K.; Liu, S.; Xing, R. Recent Developments in Air-Trapped Superhydrophobic and Liquid-Infused Slippery Surfaces for Anti-Icing Application. *Prog. Org. Coat.* **2019**, *137*, No. 105373.

(4) Cheng, Q.; Li, M.; Zheng, Y.; Su, B.; Wang, S.; Jiang, L. Janus Interface Materials: Superhydrophobic Air/Solid Interface and Superoleophobic Water/Solid Interface Inspired by a Lotus Leaf. *Soft Matter* **2011**, *7*, 5948−5951.

(5) Yin, K.; Yang, S.; Dong, X.; Chu, D.; Duan, J.A.; He, J. Ultrafast Achievement of a Superhydrophilic/Hydrophobic Janus Foam by Femtosecond Laser Ablation for Directional Water Transport and Efficient Fog Harvesting. *ACS Appl. Mater. Interfaces* **2018**, *10*, 31433−31440.

(6) Zhu, R.; Liu, M.; Hou, Y.; Zhang, L.; Li, M.; Wang, D.; Wang, D.; Fu, S. Biomimetic Fabrication of Janus Fabric with Asymmetric Wettability for Water Purification and Hydrophobic/Hydrophilic Patterned Surfaces for Fog Harvesting. *ACS Appl. Mater. Interfaces* **2020**, *12*, 50113−50125.

(7) Su, Y.; Cai, S.; Wu, T.; Li, C.; Huang, Z.; Zhang, Y.; Wu, H.; Hu, K.; Chen, C.; Li, J.; Hu, Y.; et al. Smart Stretchable Janus Membranes with Tunable Collection Rate for Fog Harvesting. *Adv. Mater. Interfaces* **2019**, *6*, No. 1901465.

(8) Cao, M.; Xiao, J.; Yu, C.; Li, K.; Jiang, L. Hydrophobic/Hydrophilic Cooperative Janus System for Enhancement of Fog Collection. *Small* **2015**, *11*, 4379−4384.

(9) Yang, H. C.; Zhong, W.; Hou, J.; Chen, V.; Xu, Z. K. Janus Hollow Fiber Membrane with a Mussel-Inspired Coating on the Lumen Surface for Direct Contact Membrane Distillation. *J. Membr. Sci.* **2017**, *523*, 1−7.

(10) Cong, S.; Guo, F. Janus Nanofibrous Membranes for Desalination by Air Gap Membrane Distillation. *ACS Appl. Polym. Mater.* **2019**, *1*, 3443−3451.

(11) Chew, N. G. P.; Zhang, Y.; Goh, K.; Ho, J. S.; Xu, R.; Wang, R. Hierarchically Structured Janus Membrane Surfaces for Enhanced Membrane Distillation Performance. *ACS Appl. Mater. Interfaces* **2019**, *11*, 25524−25534.

(12) Tian, P.; Gao, X.; Wen, G.; Zhong, L.; Wang, Z.; Guo, Z. Novel Fabrication of Polymer/Carbon Nanotube Composite Coated Janus Paper for Humidity Stress Sensor. *J. Colloid Interface Sci.* **2018**, *532*, 517−526.

(13) Zhou, H.; Wang, H.; Niu, H.; Lin, T. Superphobicity/philicity Janus Fabrics with Switchable, Spontaneous, Directional Transport Ability to Water and Oil Fluids. *Sci. Rep.* **2013**, *3*, No. 2964.

(14) Zhang, C.; He, S.; Wang, D.; Xu, F.; Zhang, F.; Zhang, G. Facile Fabricate a Bioinspired Janus Membrane with Heterogeneous Wettability for Unidirectional Water Transfer and Controllable Oil−Water Separation. *J. Mater. Sci.* **2018**, *53*, 14398−14411.

(15) Hou, L.; Wang, N.; Man, X.; Cui, Z.; Wu, J.; Liu, J.; Li, S.; Gao, Y.; Li, D.; Jiang, L.; Zhao, Y. Interpenetrating Janus Membrane for High Rectification Ratio Liquid Unidirectional Penetration. *ACS Nano* **2019**, *13*, 4124−4132.

(16) Xu, W.; Hu, X.; Zhuang, S.; Wang, Y.; Li, X.; Zhou, L.; Zhu, S.; Zhu, J. Flexible and Salt Resistant Janus Absorbers by Electrospinning for Stable and Efficient Solar Desalination. *Adv. Energy Mater.* **2018**, *8*, No. 1702884.

(17) Chen, J.; Yin, J. L.; Li, B.; Ye, Z.; Liu, D.; Ding, D.; Qian, F.; Myung, N. V.; Zhang, Q.; Yin, Y. Janus Evaporators with Self-recovering Hydrophobicity for Salt-Rejecting Interfacial Solar Desalination. *ACS Nano* **2020**, *14*, 17419−17427.

(18) Lv, B.; Gao, C.; Xu, Y.; Fan, X.; Xiao, J.; Liu, Y.; Song, C. A Self-Floating, Salt-Resistant 3D Janus Radish-Based Evaporator for Highly Efficient Solar Desalination. *Desalination* **2021**, *510*, No. 115093.

(19) Qin, D. D.; Zhu, Y. J.; Yang, R. L.; Xiong, Z. C. A Salt-Resistant Janus Evaporator Assembled from Ultra-Long Hydroxyapatite Nanowires and Nickel Oxide for Efficient and Recyclable Solar Desalination. *Nanoscale* **2020**, *12*, 6717−6728.

(20) Zhang, Q.; Yi, G.; Fu, Z.; Yu, H.; Chen, S.; Quan, X. Vertically Aligned Janus MXene-based Aerogels for Solar Desalination with High Efficiency and Salt Resistance. *ACS Nano* **2019**, *13*, 13196−13207.

(21) Gupta, P.; Kandasubramanian, B. Directional Fluid Gating by Janus Membranes with Heterogeneous Wetting Properties for Selective Oil−Water Separation. *ACS Appl. Mater. Interfaces* **2017**, *9*, 19102−19113.

(22) Li, N.; Yu, C.; Si, Y.; Song, M.; Dong, Z.; Jiang, L. Janus Gradient Meshes for Continuous Separation and Collection of Flowing Oils under Water. *ACS Appl. Mater. Interfaces* **2018**, *10*, 7504−7511.

(23) Wang, Z.; Liu, X.; Guo, J.; Sherazi, T. A.; Zhang, S.; Li, S. A Liquid-Based Janus Porous Membrane for Convenient Liquid−Liquid Extraction and Immiscible Oil/Water Separation. *Chem. Commun.* **2019**, *55*, 14486−14489.

(24) Liu, Y. Q.; Han, D. D.; Jiao, Z. Z.; Liu, Y.; Jiang, H. B.; Wu, X. H.; Ding, H.; Zhang, Y. L.; Sun, H. B. Laser-Structured Janus Wire Mesh for Efficient Oil−Water Separation. *Nanoscale* **2017**, *9*, 17933−17938.

(25) Liu, Z.; Zhang, H.; Han, Y.; Huang, L.; Chen, Y.; Liu, J.; Wang, X.; Liu, X.; Ling, S. Superaerophilic Wedge-Shaped Channels with Precovered Air Film for Efficient Subaqueous Bubbles/Jet Transportation and Continuous Oxygen Supplementation. *ACS Appl. Mater. Interfaces* **2019**, *11*, 23808−23814.

(26) Jimenez, M.; Dietrich, N.; Grace, J. R.; Hébrard, G. Oxygen Mass Transfer and Hydrodynamic Behavior in Wastewater: Determination of Local Impact of Surfactants by Visualization Techniques. *Water Res.* **2014**, *58*, 111−121.

(27) Sarkar, M. S. K. A.; Donne, S. W.; Evans, G. M. Hydrogen Bubble Flotation of Silica. *Adv. Powder Technol.* **2010**, *21*, 412−418.

(28) Kermani, M. B.; Morshed, A. Carbon Dioxide Corrosion in Oil and Gas Production Compendium. *Corrosion* **2003**, *59*, 659−683.

(29) Achilias, D.S. Studying Corrosion Electrochemical Mechanism in Tube Line and Gas Wells. *Int. J. Chem.* **2012**, *01*, 87−93.

(30) Zhang, J.; Liu, P.; Yi, B.; Wang, Z.; Huang, X.; Jiang, L.; Yao, X. Bio-Inspired Elastic Liquid-Infused Material for on-Demand Underwater Manipulation of Air Bubbles. *ACS Nano* **2019**, *13*, 10596−10602.

(31) Ma, H.; Cao, M.; Zhang, C.; Bei, Z.; Li, K.; Yu, C.; Jiang, L. Directional and Continuous Transport of Gas Bubbles on Superaerophilic Geometry-Gradient Surfaces in Aqueous Environments. *Adv. Funct. Mater.* **2018**, *28*, No. 1705091.

(32) Wang, X.; Wang, Z.; Heng, L.; Jiang, L. Stable Omniphobic Anisotropic Covalently Grafted Slippery Surfaces for Directional Transportation of Drops and Bubbles. *Adv. Funct. Mater.* **2020**, *30*, No. 1902686.

(33) Zhu, S.; Li, J.; Cai, S.; Bian, Y.; Chen, C.; Xu, B.; Su, Y.; Hu, Y.; Wu, D.; Chu, J. Unidirectional Transport and Effective Collection of Underwater CO_2 Bubbles Utilizing Ultrafast-Laser-Ablated Janus Foam. *ACS Appl. Mater. Interfaces* **2020**, *12*, 18110−18115.

(34) Duan, J. A.; Dong, X.; Yin, K.; Yang, S.; Chu, D. A Hierarchical Superaerophilic Cone: Robust Spontaneous and Directional Transport of Gas Bubbles. *Appl. Phys. Lett.* **2018**, *113*, No. 203704.

https://doi.org/10.1021/acsami.2c12027
ACS Appl. Mater. Interfaces XXXX, XXX, XXX−XXX

(35) Yu, C.; Zhang, P.; Wang, J.; Jiang, L. Superwettability of Gas Bubbles and its Application: from Bioinspiration to Advanced Materials. *Adv. Mater.* **2017**, *29*, No. 1703053.
(36) Yin, K.; Yang, S.; Dong, X.; Chu, D.; Gong, X.; Duan, J. A. Femtosecond Laser Fabrication of Shape-Gradient Platform: Underwater Bubbles Continuous self-Driven and Unidirectional Transportation. Appl. *Surf. Sci.* **2019**, *471*, 999−1004.
(37) Gao, A.; Fan, H.; Zhang, G.; Zhao, S.; Cui, J.; Yan, Y. Facile Construction of Gas Diode Membrane Towards in Situ Gas Consumption via Coupling Two Chemical Reactions. *J. Colloid Interface Sci.* **2019**, *557*, 282−290.
(38) Hu, Y.; Qiu, W.; Zhang, Y.; Zhang, Y.; Li, C.; Li, J.; Wu, S.; Zhu, W.; Wu, D.; Chu, J. Channel-Controlled Janus Membrane Fabricated by Simultaneous Laser Ablation and Nanoparticles Deposition for Underwater Bubbles Manipulation. *Appl. Phys. Lett.* **2019**, *114*, No. 173701.
(39) Wang, G. J.; Wu, B. H.; Xu, Z. K.; Wan, L. S. Janus Polymer Membranes Prepared by Single-Side Polydopamine Deposition for Dye Adsorption and Fine Bubble Aeration. *Mater. Chem. Front.* **2019**, *3*, 2102−2109.
(40) Pei, C.; Peng, Y.; Zhang, Y.; Tian, D.; Liu, K.; Jiang, L. An Integrated Janus Mesh: Underwater Bubble Antibuoyancy Unidirectional Penetration. *ACS Nano* **2018**, *12*, 5489−5494.
(41) Chen, C.; Shi, L. A.; Huang, Z.; Hu, Y.; Wu, S.; Li, J.; Wu, D.; Chu, J. Microhole-Arrayed PDMS with Controllable Wettability Gradient by One-Step Femtosecond Laser Drilling for Ultrafast Underwater Bubble Unidirectional Self-Transport. *Adv. Mater. Interfaces* **2019**, *6*, No. 1900297.
(42) Lee, J.; Kim, J.; Kim, H.; Bae, Y. M.; Lee, K. H.; Cho, H. J. Effect of Thermal Treatment on the Chemical Resistance of Polydimethylsiloxane for Microfluidic Devices. *J. Micromech. Microeng.* **2013**, *23*, No. 035007.
(43) Sankır, M.; Küçükyavuz, Z.; Küçükyavuz, S. Synthesis and Characterization of Poly (Dimethylsiloxane)−Polythiophene Composites. *J. Appl. Polym. Sci.* **2003**, *87*, 2113−2119.
(44) Chang, M. J.; Cui, W. N.; Chai, X. J.; Liu, J.; Wang, K.; Qiu, L. Fabrication of Flexible MIL-100 (Fe) Supported SiO_2 Nanofibrous Membrane for Visible Light Photocatalysis. *J. Mater. Sci.* **2019**, *30*, 1009−1016.
(45) Schnyder, B.; Lippert, T.; Kötz, R.; Wokaun, A.; Graubner, V. M.; Nuyken, O. UV-Irradiation Induced Modification of PDMS Films Investigated by XPS and Spectroscopic Ellipsometry. *Surf. Sci.* **2003**, *532*−*535*, 1067−1071.
(46) Brunet, P.; Lapierre, F.; Thomy, V.; Coffinier, Y.; Boukherroub, R. Extreme Resistance of Superhydrophobic Surfaces to Impalement: Reversible Electrowetting Related to the Impacting/Bouncing Drop Test. *Langmuir* **2008**, *24*, 11203−11208.
(47) Nhung Nguyen, T. P.; Brunet, P.; Coffinier, Y.; Boukherroub, R. Quantitative Testing of Robustness on Superomniphobic Surfaces by Drop impact. *Langmuir* **2010**, *26*, 18369−18373.
(48) Gurera, D.; Bhushan, B. Bioinspired Movement of Gas Bubbles: Composition, Applications, Generation, Contact Angle, and Movement−an Overview. *Mol. Syst. Des. Eng.* **2020**, *5*, 1555−1577.
(49) Tahzibi, H.; Azizian, S. Fabrication of Superhydrophobic-icephobic Carbon Cloth using Polydimethylsiloxane for Oil−Water Separation. *J. Mol. Liq.* **2022**, *356*, No. 119008.

https://doi.org/10.1021/acsami.2c12027
ACS Appl. Mater. Interfaces XXXX, XXX, XXX−XXX